Experimental and numerical investigation of V-bent anisotropic 304L SS sheet with spring-forward considering deformation-induced martensitic transformation

Masoud Ahmadi [a], Bagher Mohammad Sadeghi [a,*], Hossein Arabi [b]

[a] School of Metallurgy and Materials Engineering, Iran University of Science and Technology, Tehran, Iran
[b] Center of Excellence for High Strength Alloy Technology, School of Metallurgy and Materials Engineering, Iran University of Science and Technology, Tehran, Iran

HIGHLIGHTS

- Spring-forward of 304L steel sheet was examined using a novel V-bending die and verified by finite element analysis.
- Martensitic transformation was affected by austenite grain size and orientation, deformation mode and anisotropy factor.
- An empirical equation was proposed to correlate residual magnetic field and fraction of transformed α'-martensite.
- The amount of spring-forward increased by raising the fraction of α'-martensite in V-bent samples.

GRAPHICAL ABSTRACT
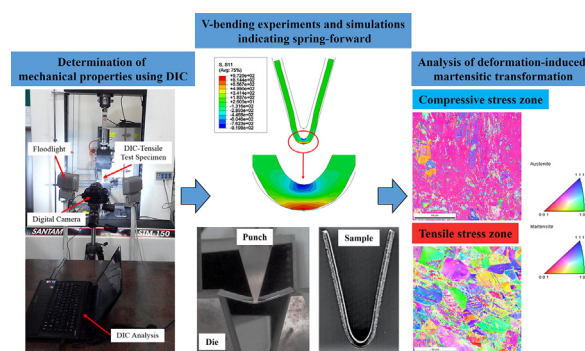
ARTICLE INFO

ABSTRACT

Spring-back/forward phenomenon usually occurs during various kinds of bending tests of sheet metals. In this study, using a digital image correlation (DIC) technique coupled with uniaxial tensile test, mechanical properties of AISI 304L austenitic stainless steel were determined and the results were applied into finite element analysis (FEA) for further investigations. In order to examine various parameters affecting spring-forward in V-bending, a novel V-bending die equipped with data acquisition system was designed and used to perform V-bending tests of the AISI 304L stainless steel samples. For investigating crystallographic texture evolution in the bent sample, electron backscatter diffraction (EBSD) analysis was conducted. Furthermore, microstructural characterization, micro-hardness test and residual magnetic field measurement were utilized to investigate the transformation of austenite to α'-martensite in the bent samples. The results revealed that spring-forward angle raised by increasing sample thickness and lowering bending angle and anisotropy parameter. The fraction of transformed α'-martensite was affected by mode of deformation (stress state). An empirical model was suggested to relate residual magnetic field to volume fraction of α'-martensite for bent samples. In order to control the spring-forward efficiently, the contribution of microstructural evolution in V-bent samples was discussed.

© 2017 Elsevier Ltd. All rights reserved.

* Corresponding author at: School of Metallurgy and Materials Engineering, Iran University of Science and Technology, Narmak, Tehran, Iran.
E-mail addresses: masoud.ahmadi@bilkent.edu.tr (M. Ahmadi), bmsadeghi@iust.ac.ir (B. Mohammad Sadeghi), arabi@iust.ac.ir (H. Arabi).

1. Introduction

Dimensional accuracy is highly regarded in manufacturing science and industry to avoid further product defects exploited in different applications. In order to fabricate metallic parts in sheet metal forming industries, spring-back/forward phenomenon should be taken into consideration. During various types of bending tests including L-bending, U-bending, Z-bending and V-bending, spring-back/forward may occur as a function of process and material properties parameters. Upon unloading, at the end of the loading imposed to a sheet metal in bending tests, the sheet metal exhibits relaxation and recovery of the applied strain. This may cause the specimen to have dimensional alterations which may appear in spring-back or spring-forward format [1–6].

Spring-back occurs when the angle of the bent sheet sample exceeds that of the die, however, spring-forward (also known as spring-go) happens if the angle of the sheet sample becomes lower than that of the die under special circumstances including small die radius [7]. These critical phenomena have been studied by many researchers from different aspects. For instance Levy [8] investigated different die geometries and proposed an empirical equation to predict spring-back on the basis of specimen and die parameters. Zhang et al. [9] studied V-bending using deformable punches and confirmed the occurrence of spring-forward. Chan et al. [10] developed a finite element method (FEM) to address the effect of punch radius, punch angle and die-lip radius. Thipprakmas [11] also utilized FEM and experiments considering sided coined-bead technique to manage the spring-forward. A more detailed microstructural based study was performed by Chatti and Fathallah [12]. They claimed that for small plastic strain, the reduction of elastic modulus can be attributed to the dislocations structure affecting spring-back. Duc-Toan et al. [13] also evaluated a FE simulation in order to model spring-back behavior of a magnesium alloy at various temperatures. To validate the experimental results, kinematic/isotropic hardening law was utilized and combined with a modified Johnson-Cook model and implemented into their simulation procedure. Leu [4] reported an experimental and FEM study to evaluate the spring-back/forward of high strength steel sheet samples in V-die bending experiment with asymmetric dies. The results highlighted that large sheet thickness and low friction have positive effect on incidence of spring-forward.

Austenitic stainless steels (ASSs) are acknowledged by their wide range of applications in automotive and home appliance manufacturing and metal forming industries. Due to the high strength, excellent formability and unique corrosion resistance, many researchers have investigated austenitic stainless steels in their studies [14–16]. These alloys contains low carbon and high amounts of chromium and nickel. When austenitic stainless steels are subjected to mechanical forces, metastable austenite (FCC) phase tends to transform to α'-martensite (BCC) phase. This process is known as the transformation induced plasticity (TRIP) phenomenon. Stacking fault energy (SFE) and composition of the alloy are said to have the most significant role in mechanism of austenite to martensitic phase transformation [17,18]. Moreover, the kinetics of solid state phase transformation of austenite to α'-martensite was first modeled by Olson and Cohen [19]. This model expresses that the amount of α'-martensite nucleation is a function of imposed plastic strain and temperature.

The transformation induced plasticity of austenitic stainless steel has been observed and utilized in previous literature. For example, Karimi et al. [20] and Hedayati et al. [21] distinctively reported the mechanically induced phase transformation of 304L stainless steel during cold rolling. In the latter research, the results revealed that extent of measured transformed α'-martensite resulted from rolling experiments were found in accordance with Olson-Cohen [19] model. Recently Wang et al. [22] performed a more detailed research focusing on crystallographic issues during 304 stainless steel under tension. A phase transformation crystal plasticity model was recommended to gain a profound understanding about austenite to martensite phase transformation and texture development. Fei and Hodgson [23] used TRIP

steel in their investigation in air V-bending tests and evaluated influence of blank thickness, Young's modulus and die gap on spring-back. However, the microstructural issues were not studied extensively in their research. Shan et al. [24] considered the martensitic phase transformation in deep drawing operation and reported that spring-back was affected by TRIP phenomenon and variation of Young's modulus in austenitic steel deep drawn parts. For V-bending process considering microstructural evolution, one of the rare works was performed by Kim and Lee [25]. They carried out bending tests on different TRIP samples with various amounts of retained austenite after performing heat treatments. They reported the effect of martensitic transformation on spring-back/forward. However, a profound stress/strain based quantification of martensitic transformation, analysis of deformation modes and crystallographic texture evaluations on the bent samples were not encompassed in their study.

Based on the aforementioned studies, as well as the conventional parameters affecting spring-forward, this research work aims to conduct a comprehensive investigation to make a correlation between texture/microstructural evolution and spring-forward phenomenon, including stress/strain martensitic transformation quantification in V-bent anisotropic TRIP steel. For this purpose, a novel V-bending die was fabricated and utilized in order to analyze spring-forward phenomenon of AISI 304L stainless steel sheet metals combined with austenite to α'-martensite phase transformation. In addition, EBSD analysis, microstructural characterization, residual magnetic field and microhardness evaluations were also conducted to study the relevant issues in V-bending experiments.

2. Experimental and simulation procedure

In this research, three sheets of AISI 304L fully austenitic stainless steel with thickness of 0.5 mm, 1 mm and 1.5 mm, containing the same nominal composition were used. The average chemical composition of the as-received AISI 304L stainless steel sheets are listed in Table 1. In order to prepare samples for uniaxial tensile tests, the sheets were cut in three different directions, 0° relative to rolling direction (RD), 45° from the rolling direction (QD) and 90° from the rolling direction, i.e. transverse direction (TD), according to ASTM-E8 standard [26]. Uniaxial tensile tests were performed via universal STM-150 testing machine equipped with extensometers. In order to examine the extent of anisotropy in the sheet metals, a digital image correlation (DIC) technique was manipulated to get access to strain distribution within the specimen under tensile test. The setup of DIC method assembled with tensile test machine is illustrated in Fig. 1(a), and also Fig. 1(b) shows a black speckle pattern on the surface of the DIC-tensile specimen which was painted with white color. In order to obtain strain values across the width and the length of the specimens, DIC photographs were taken in every 5 s intervals using a digital camera. The results were analyzed by a DIC MATLAB code.

Samples with the dimension of 50 × 20 mm were cut from the three sheets for bending tests. Then the bending samples were labeled according to the sheet thickness, cut direction and bending angle. For

Table 1
Mean composition of the as-received alloy.

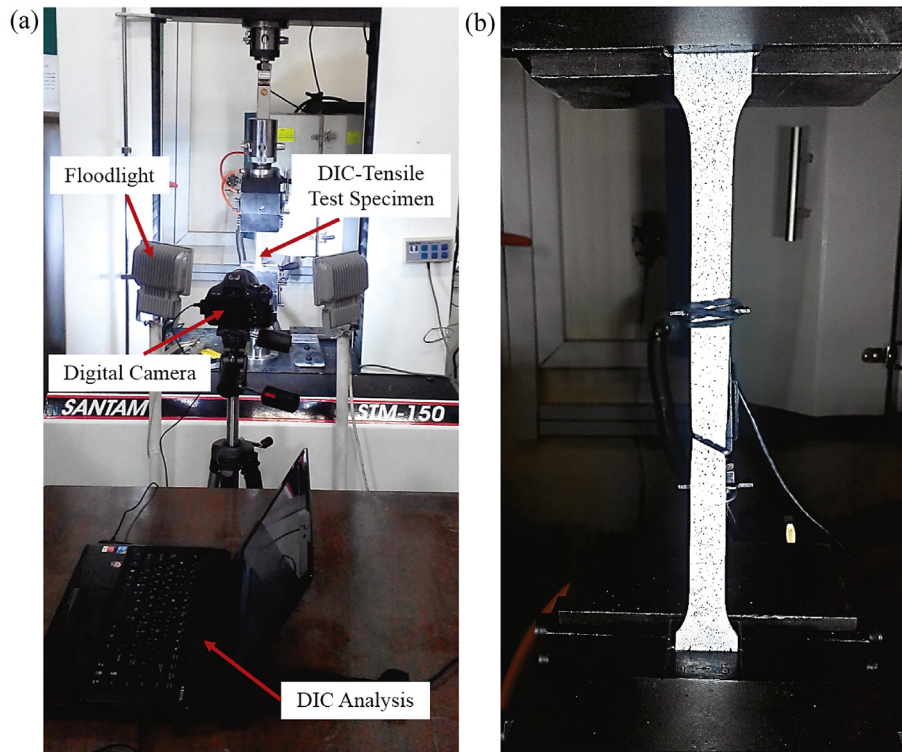| Element	(wt%)
Fe	Bal.
Cr	17.09
Ni	7.54
Mn	1.54
Si	0.49
Cu	0.28
Mo	0.2
P	0.06
Nb	0.03
C	0.01

Fig. 1. (a) DIC setup coupled with tensile test; (b) DIC-tensile specimen.

instance, 1.5TD30 code corresponds to a bending sample having 1.5 mm thickness, cut in transverse direction and bent by 30°.

In this research, a novel V-bending die equipped with data acquisition system was designed and fabricated to perform bending tests. Fig. 2 demonstrates schematic view of the experimental V-bending setup including die and punch with detailed dimensions. The die was made of carburized steel with the dimensions of 250 × 150 × 50 mm which exhibits data acquisition system and four different bending angles of 30°, 45°, 60° and 90°. One of the advantages of the proposed V-bending die is the potential to conduct bending tests for various sheet metal thicknesses from 0.1 mm to 2 mm. Consequently, V-bending tests were performed three times for each of the similar samples using the fabr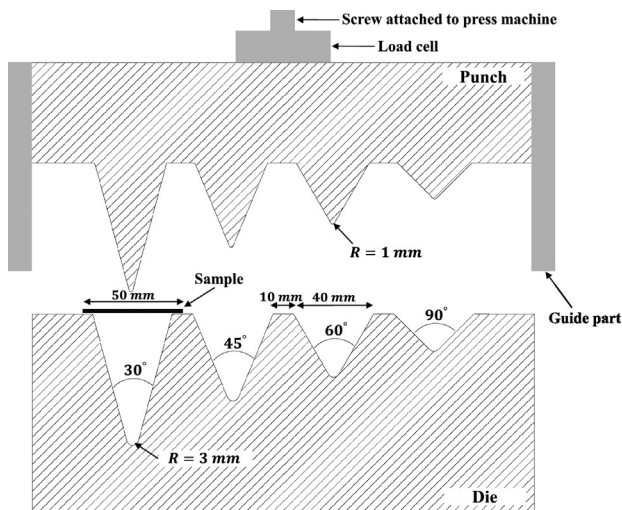icated die which was assembled on a 300 kN universal press machine, with constant speed of 10 mm/min. The tests were carried out at room temperature without any lubricant.

In order to scrutinize the texture and microstructural development in a bent sample, electron backscatter diffraction (EBSD) analysis was employed using orientation imaging microscopy (OIM) tool. The 1.5RD45 as a typical bent sample was selected for this purpose. The sample cross section was ground and polished using 0.1 μm diamond paste and then electropolished using a solution containing 4% Perchloric acid in 96% Ethanol at 40 V, for 10 s to improve the indexing of lattice orientations. It should be mentioned that, for the tensile stress zone analysis, a region between point numbers 4 and 5, and for the compressive zone, a region between point numbers 1 and 2 across the cross section (shown in Fig. 3), were selected for EBSD investigation. In EBSD analysis procedure, 20 kV accelerating voltage, 10 mm working distance and 0.2 μm step size were applied. The obtained results were analyzed by means of OIM analysis software.
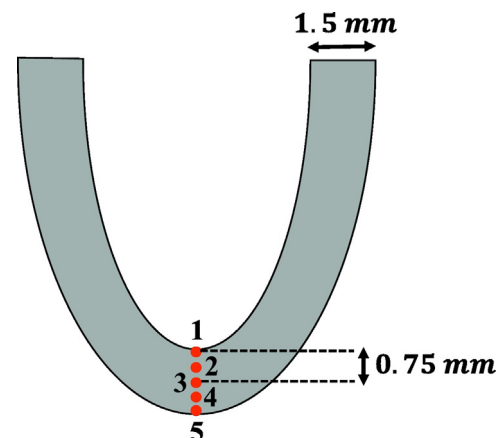

Fig. 2. Schematic view of the experimental V-bending setup including cross sections of the V-bending die and punch with detailed dimensions.

Fig. 3. Cross-sectional schematic view of a bent sample.
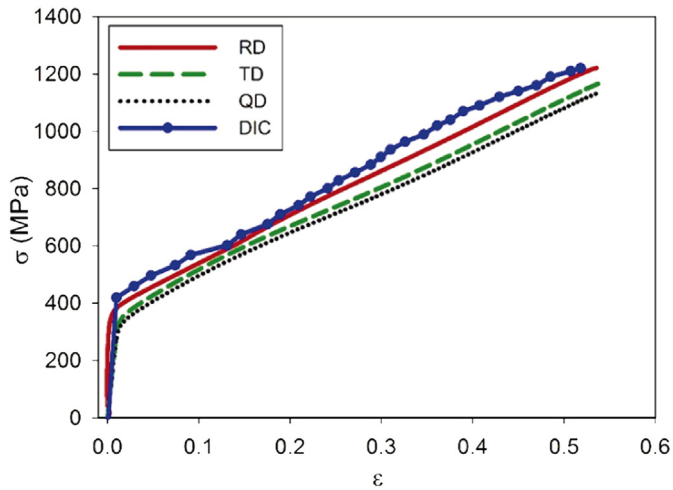
Fig. 4. Variation of true stress vs. true strain of 1.5 mm thick specimens together with the results obtained from DIC.

As a non-destructive test, magnetic field strength meter (Deutrometer 3873) was used to evaluate residual magnetic field along the bent specimens. For this purpose, the samples were initially subjected to an external magnetic field produced by a Deutropuls commercial device equipment. Afterward, residual magnetic field was measured using Deutrometer probe for 1.5 mm thick bent specimens at the outer surface in the vicinity of point number 5 demonstrated in Fig. 3.

Microstructural characterization was also carried out via a conventional metallography rout. For this purpose, bent samples were first ground and then polished using 1 μm alumina suspension solution on the nap cloth. Etching was done by a mixture of two solutions; one containing 0.2 g sodium metabisulfite in 100 ml distilled water and the other contained 10 ml hydrochloric acid in 100 ml distilled water. Consequently, microstructure characterization and Vickers micro-hardness tests were conducted on the selected V-bent samples along the point number 1 to 5 across the cross section presented in Fig. 3.

Exploiting the flow properties obtained from uniaxial tensile tests, a finite element (FE) analysis was carried out in order to predict general V-bending behavior of AISI 304L stainless steel samples. The simulations were executed in dynamic explicit mode of FEM commercial software ABAQUS™ and the obtained results were evaluated by the experimental outputs. The boundary conditions were as follows: The punch and die
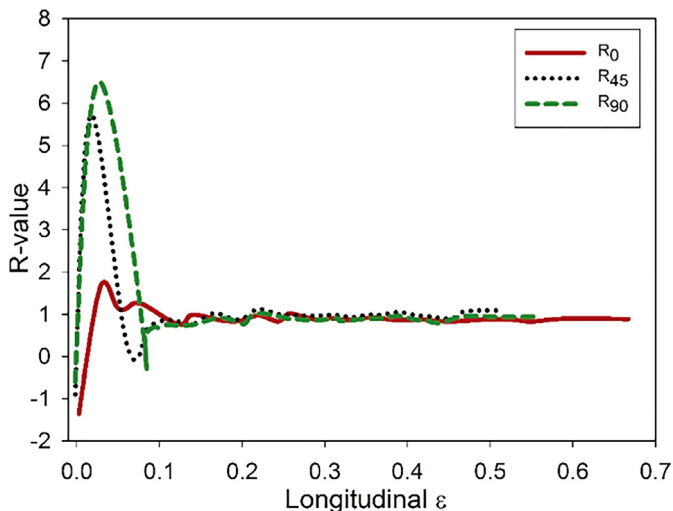
were considered rigid and the samples were set deformable, analogous to the real conditions of the performed experiments. Appropriate punch displacements were applied for every bending angle relative to the height of the corresponding die groove according to Fig. 2. Considering accuracy and time of the simulations, an optimum mesh size of 0.37 mm was selected.

3. Results and discussion

3.1. Mechanical properties

The true flow curves for RD, QD and TD 1.5 mm thick samples obtained from uniaxial tensile tests are shown in Fig. 4. Moreover, in order to validate the digital image correlation (DIC) technique in the present research, the RD sample flow curve obtained by DIC method was compared to that obtained via the extensometer illustrated in Fig. 4. The flow curve related to RD specimen is located above those of other directions and there is a slight difference in strain hardening rate for different directions of the tensile samples. Similar results were also reported in the literature for 304 stainless steel [27].

Thus, the results attained by DIC indicate that this method can be applied to gain a proper access to strain distribution along the width and length of the specimen. With the assumption of incompressibility, the plastic strain ratios (R-value) of the specimens were determined using the following equation [28]:

$$R = \frac{\varepsilon_w^p}{\varepsilon_t^p} = \frac{\varepsilon_w^p}{-(\varepsilon_w^p + \varepsilon_l^p)} \qquad (1)$$

where ε_w^p, ε_t^p and ε_l^p are plastic strains in width, thickness and length of tensile specimens respectively. Utilizing images attained from DIC method, R-values were calculated for 1.5 mm thick tensile specimens and plotted versus longitudinal strains shown in Fig. 5. Based on this figure, once the curves reached the steady state region, R-value was determined for each direction. Moreover, the mean R-value ($\bar{R}$) was also calculated as follows [28]:

$$\bar{R} = \frac{R_0 + 2R_{45} + R_{90}}{4} \qquad (2)$$

where R_0, R_{45} and R_{90} are plastic strain ratios or anisotropy parameters relative to rolling direction, i.e. RD, QD and TD respectively. The mean stress-strain curve data and anisotropy parameters for 1.5 mm thick specimens are provided in Table 2.

In order to achieve an accurate model for work hardening behavior of AISI 304L stainless steel, the plastic deformation zone of the RD specimen was selected for performing curve fitting in MATLAB software. Fig. 6 illustrates two work hardening equations compared to experimental results of the material work hardening. The results of curve fittings are provided in Table 3. Based on these results, Ludwik model fits better to stress-strain data with the R-square of 0.9997. These results are in good agreement with the literature [29]. K and n in Hollomon and Ludwik models depend on thermomechanical history and phase distribution of the alloys. Thus, due to instability of austenitic steels during plastic deformation, common Hollomon model fails to describe plasticity of AISI 304L stainless steel. Therefore, Ludwik equation as an isotropic model was selected to be implemented into finite element analysis

Fig. 5. Variation of anisotropy parameters vs. longitudinal strain of 1.5 mm thick specimens.

Table 2
Results of tensile tests and DIC of 1.5 mm thick specimens.

Direction	RD (0°)	QD (45°)	TD (90°)
Yield strength (MPa)	358.5	338	342
UTS (MPa)	1212.5	1132	1176
R-value	0.81	0.92	0.85
$\bar{R}$	0.875		
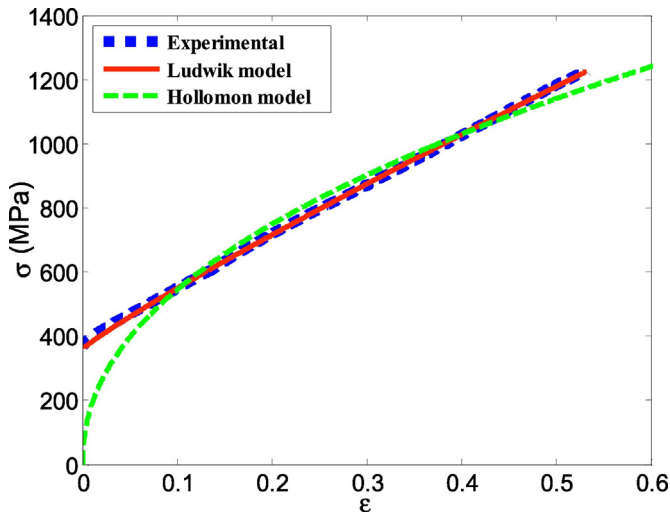
Fig. 6. Curve fitting on plastic deformation region of flow curve of RD specimen.

Fig. 7. Variation of force vs. displacement for various bent samples.

as the plastic work hardening behavior of AISI 304L stainless steel for V-bending test simulations.

3.2. Bending behavior and simulation validation

Typical force-displacement curves for four different 1.5 mm thick bent samples are illustrated in Fig. 7. The curves in Fig. 7 display similar characteristics and trends for various bending samples. The sample bent by 30° displaced more by bending force than those of the other samples possibly due to geometry of the die grooves and the steeper slopes of the groove walls which can cause a reduction in the amount of friction. In fact, since no lubrication was used in these experiments, every bending angle can alter friction coefficient by different amounts between the sample and the die. Hence, the sleeper the groove wall up to a certain amount, the lower the coefficient of friction. It is worth mentioning that, the force-displacement behavior of the bent samples is usually considered a function of geometry of the die. Therefore, in order to avoid the variation of friction coefficient in analyzing force-displacement curves more accurately, the curve for the sample bent by 45° was compared to the curve obtained from FE simulation as shown in Fig. 8. The curve obtained by FE simulation is highly analogous to that of experimental test which is an indication of the validity of bending simulations in the current work.

Force-displacement curves depicted in Fig. 8 were divided into 4 regions in order to interpret the mechanical behavior of the samples under bending. In the first region, the change in displacement considered linear with increasing force, whereas, in the second region by increasing force, displacement raised but with a decelerating rate. Then with further displacement in the third region no considerable change in force was observed and finally, the rate of changing force was accelerated with displacement in the fourth region. Region 1 corresponds to elastic properties of the sample. At the end of the first region, mobile dislocations on the slip planes start to move but due to their interactions, the rate of deformation decreased to a minimum value at the second region and then remained constant at the third region. At the beginning of the third region, sliding has occurred where the tip of the punch was in contact with the sheet sample. In the fourth region which is the final stage of bending, sample surface was almost in full
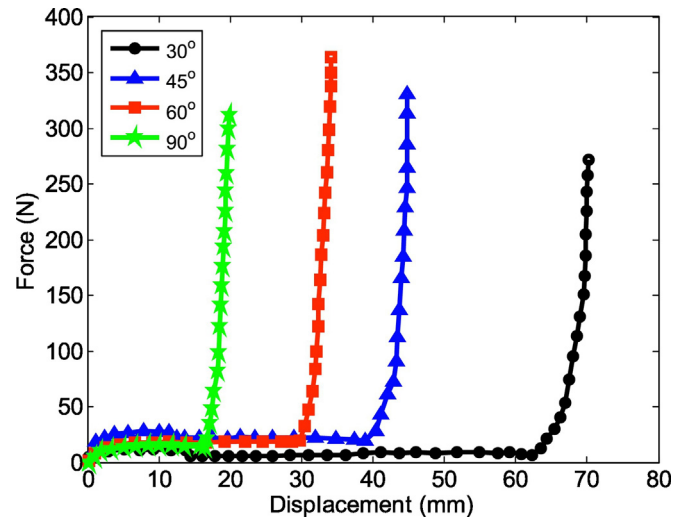
contact with the punch and the die surfaces. At the onset of this region known as coining region [9] and designated by C in Fig. 8, plastic deformation started increasing rapidly with an accelerating rate.

After conducting V-bending tests three times for each sheet, the mean angle of the bent samples were measured using ImageJ software. As it is demonstrated in Fig. 9, all the angles of bent samples found experimentally were lower than those of the corresponding die groove. These results indicate that spring-forward (negative spring-back) phenomenon occurred in the bent samples due to the sharp radius of the punch tip, as it has also been reported in the literature [32]. Furthermore, the predicted angles of samples after V-bending simulations agree well with experimental results shown in Fig. 9. It is worth mentioning that, in the present study, simulations were performed to generally predict V-bending behavior of the samples with respect to mechanical properties obtained for rolling direction of the specimens,
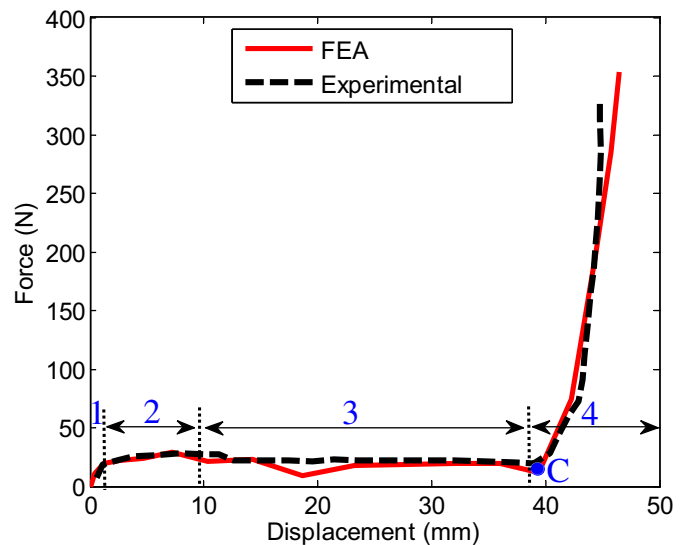

Fig. 8. Variation of force vs. displacement for 1.5RD45 sample compared to FEA results.

Table 3
Comparison of selected work hardening models.

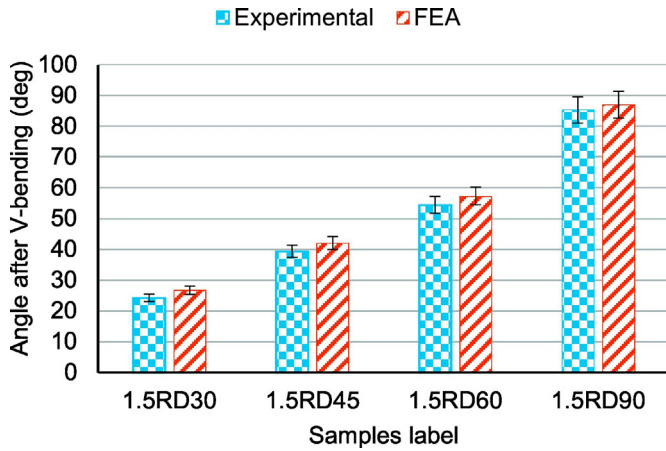| Work hardening model	Work hardening equation	Strength coefficient/K(MPa)	Strain hardening exponent/n	Yield stress/σ_y(MPa)	R^2
Hollomon [30]	$\sigma = K\varepsilon^n$	1565	0.46	–	0.9558
Ludwik [31]	$\sigma = \sigma_y + K\varepsilon^n$	1537	0.9	358	0.9997

Fig. 9. Average angles of bent samples compared to FEA.

(a)

however, the effect of anisotropy of the sheets was not considered in the simulation stage.

Stress and strain distributions along the cross section of the 1.5RD30 bent sample resulted from FE analysis and presented in Fig. 10, were used to elaborate spring-forward phenomenon. This figure shows that the bent sample exhibits two regions with different stress states along its cross section. Fig. 10(a) shows that the zone which was in contact with punch tip experienced compressive force and the region next to the die surface experienced tensile force. The surface areas of the stated zones play a significant role in spring-back/forward phenomenon. In the utilized V-bending die, since the punch tip radius was smaller than the die radius, the punch tip penetrated the neutral axis during thinning of the sample at the bending point. Thus, the compressive zone became the dominant region, however, the maximum absolute value of stress in tensile zone was greater (972 MPa) than that of compressive zone (919.9 MPa).

During unloading both tensile and compressive zones tended to recover the imposed elastic strains where compressive zone surpassed the tensile region. It is worth noticing that, at the mid plane of the cross section known as neutral axis, the value of stress becomes zero while the amount of strain is not zero as indicated in Fig. 10(b). This figure indicates that the maximum equivalent plastic strain was obtained in the outer surface of the sample where it was in contact with the die.

In the current research, the magnitude of the spring-forward angle (α_{SF}) has been defined simply as the following [5]:

$$\alpha_{SF} = \alpha_d - \alpha_b \qquad (3)$$

where α_d is the angle of the die and α_b is the angle of the bent sample. The average amount of α_{SF} for different labeled samples are given in Fig. 11. This figure indicates that by increasing the bending angle in almost all of the samples undergone bending tests, the magnitude of spring-forward decreased accordingly. This may be attributed to the fact that smaller bending angle enhances the contact area of compressive force which was discussed earlier in this research.

Fig. 11 also shows by increasing the thickness of the sheet samples from 0.5 mm to 1.5 mm, α_{SF} increased in almost all cases except in 0.5RD90 sample for which the value of α_{SF} was higher than that of 1RD90. This might be due to possible alteration of strain rate or imposed loading time as well as some inhomogeneities in the microstructure of this sample. One should note that, the rise in thickness caused an increase in cross-sectional area of the specimens. This resulted to more plastic deformation imposed by the punch tip which subsequently can increase the amount of residual stress within the specimen leading to higher α_{SF}. Moreover, this outcome may be attributed to reduction of clearance angle between the punch and the die as the result of enlarging
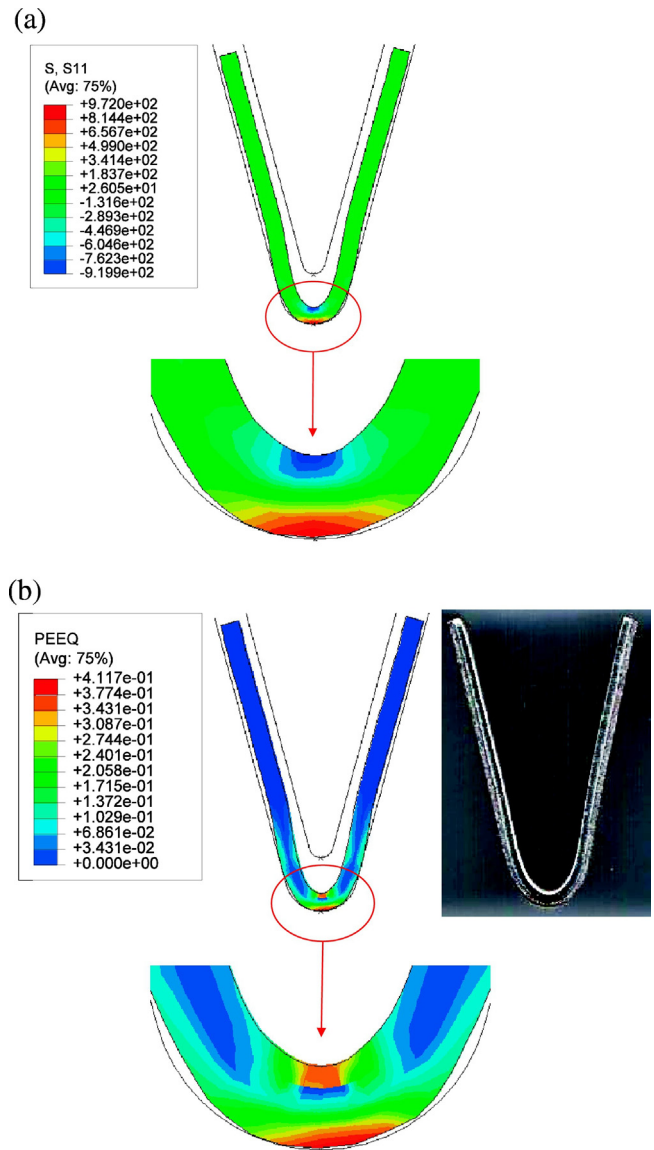
(b)

Fig. 10. (a) Distribution of stress along the cross section of 1.5RD30 sample; (b) Distribution of equivalent plastic strain compared to experimental 1.5RD30 bent sample.

sample thickness. The discussed observation highly agrees with studies reported by Thipprakmas [33] for V-bending dies and recently by Leu [34] using an analytical approach for U-bending dies.
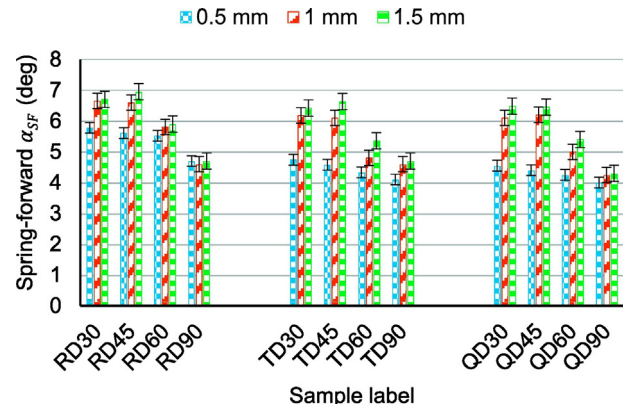

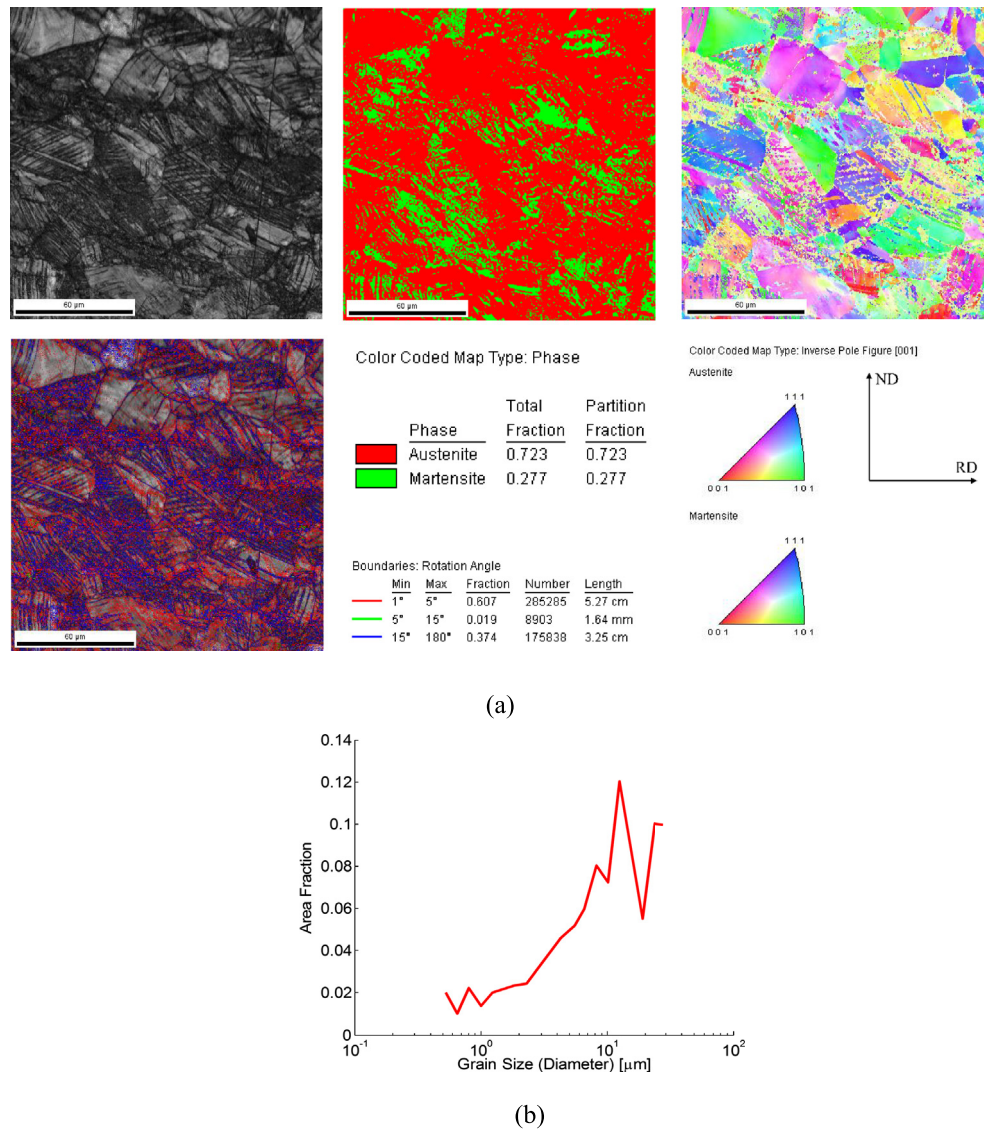Fig. 11. Average spring-forward angles of all bent samples.

(a)

(b)

Fig. 12. (a) EBSD maps of the tensile stress zone for 1.5RD45 bent sample; (b) Corresponding austenite grain size variation.

Variation of anisotropy (R-value) was also considered as a crucial parameter affecting spring-forward behavior of the samples. Comparing the results of α_{SF} obtained for different directions of the bent samples (Fig. 11) reveals that RD samples exhibit slightly higher α_{SF} than other orientations. The amounts of spring-forward for TD samples were also generally higher than those of QD samples. These differences are very noticeable for the variation of anisotropy parameters (R-values) in each sample. R-values are given in Table 2 show RD samples exhibiting the lowest anisotropy (i.e. lower R-value) have the highest α_{SF} compared to α_{SF} of TD and QD samples as shown in Fig. 11.

These results provide a precise and useful insight for manufacturer of stainless steel products to consider the spring-forward phenomenon during die designing stage. For instance, based on α_{SF} results obtained for 0.5RD30 sample shown in Fig. 11, and considering the configuration of the proposed V-bending die, if it is intended to produce a final 30° V-shaped sample with 0.5 mm thickness cut in rolling direction, instead of designing a 30° bending die, a die with bending angle of 35.7° (i.e. the sum of intended sample angle (30°) and spring-forward value (5.7°)) should be used to compensate for the spring-forward phenomenon.

3.3. Texture and microstructural evolution

In order to analyze the influence of V-bending on crystallographic texture and microstructural evolution in the bent samples, 1.5RD45 as a typical bent sample was selected for electron backscatter diffraction (EBSD) analysis in the regions discussed in Section 2. Orientation color maps and austenite grain size variation of the tensile and compressive stress zones attained from EBSD results are provided in Figs. 12 and 13 respectively.

Fig. 12(a) shows the fraction of transformed α'-martensite (having BCC structure) in the tensile stress zone was 0.277, whereas, the amount of transformed α'-martensite was found as 0.217 for the compressive zone illustrated in Fig. 13(a). According to Lebedev [35] deformation by tension promotes austenite to α'-martensite transformation, on the contrary, deformation caused by compression can reduce this type of transformation substantially.

It is worth mentioning that, since mechanical properties of austenitic stainless steels are mainly affected by austenite to α'-martensite transformation [36], in the present study, the formation of ϵ-martensite (having HCP structure) has not been taken into account. According to Gey et al. [37] the martensitic transformation rate in austenitic stainless
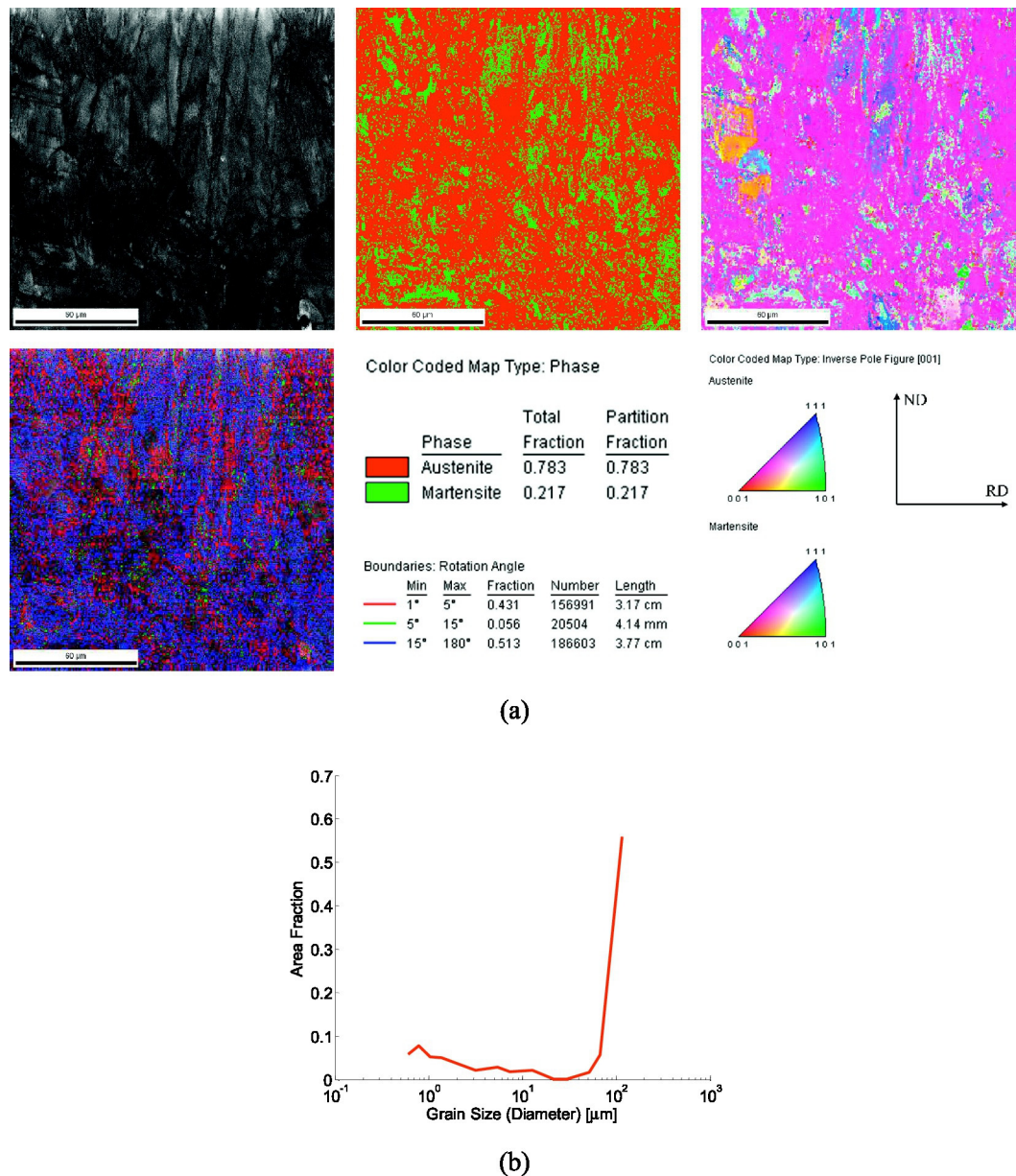
Fig. 13. (a) EBSD maps of the compressive stress zone for 1.5RD45 bent sample; (b) Corresponding austenite grain size variation.

steel depends on orientation and size of the parent austenite grains. Austenite grain size distribution for tensile and compressive zones are presented in Fig. 12(b) and Fig. 13(b) respectively. One should notice that, in the tensile zone the size of the equiaxed austenite grains varies between 0.5 μm and 30 μm which is less than the size range of elongated grains in compressive zone, i.e. 0.5 μm–100 μm. The smaller grain size together with the higher numbers of austenite grains in tensile zone compared to compressive zone, promote the number of favorable habit planes within the microstructure [38] for occurrence of austenite to α′-martensite transformation which consequently increases the volume fraction of α′-martensite. Similar observations have been reported in the previous research works [37,39].

By comparing Fig. 12(a) and Fig. 13(a), one can observe that the developed microstructures for tensile and compressive zones are essentially different. In the compressive zone, most of austenite grains (purple color) are oriented to approximately [112] direction, whereas, in the tensile zone austenite grains are not oriented in any particular direction. These results are in fair agreement with the recent investigations on austenitic stainless steels [40,41]. Moreover, as illustrated in

Fig. 12(a) and Fig. 13(a), the α′-martensite grains in the tensile zone are diversely oriented, whereas, in the compressive zone they are aligned mostly to the normal direction (ND) of the bent sample. These figures also depict that, for the tensile stress zone the low angle grain boundaries (LAGBs), i.e. angles between 1° and 15° surpass the high angle grain boundaries (HAGBs), i.e. angles between 15° and 180°, whereas, for the compressive stress zone HAGBs exceed LAGBs. These observations are mainly due to the fact that, in the compressive stress zone the sample which was in contact with the sharp punch tip, experienced more localized plastic deformation as the result of more penetration of punch tip to the neutral axis during sample thinning.

In order to evaluate the fraction of the transformed α′-martensite for different bent samples in a more convenient way, in addition to EBSD, several optical micrographs of the tensile and compressive zones were also taken from 1.5 mm thick bent samples. Typical micrographs of 1.5RD30 have been presented in Fig. 14. The darker regions in these micrographs correspond to α′-martensite phase and the remaining light regions are austenite phase. It is said [42] that the nucleation of α′-martensite having BCC structure normally occurs at shear bands which
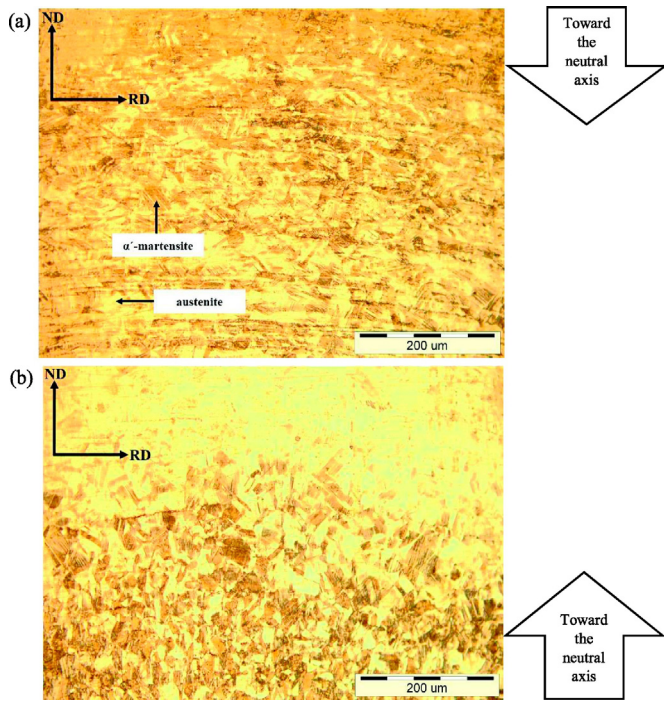
Fig. 14. Optical micrograph of 1.5RD30 sample for (a) Tensile stress zone; (b) Compressive stress zone.

Fig. 15. Variation of equivalent plastic strain along the cross section of bent samples.

form during plastic deformation. As Fig. 14(a) depicts, α'-martensite phases are roughly oriented along the length of the sample in tensile stress zone, while in the compressive zone shown in Fig. 14(b), α'-martensite phase are aligned to the normal direction (ND) which was also observed in EBSD results. Therefore, one may say that, shear bands formation and subsequently α'-martensite transformation can be influenced by the nature of the induced stress within the specimen.

Apparently, by moving from edge of the tensile or compressive zones toward the neutral axis of the bent sample, the amount of α'-martensite decreased as shown in Fig. 14 (i.e. less darker regions appeared).

Volume fraction of α'-martensite was also measured by means of microstructural image analysis utilizing ImageJ software for 1.5RD30, 1.5RD45, 1.5RD60 and 1.5RD90 bent samples. The results of image analysis are presented in Table 4 for both compressive stress and tensile stress zones. Volume fraction of α'-martensite was higher in tensile stress zone than in compressive zone. This was also discussed earlier in EBSD analysis. Comparing the results of Table 4 with Fig. 12(a) and Fig. 13(a) for 1.5RD45 sample, one may notice that volume fraction of α'-martensite in tensile zone was 0.29 when using image analysis, and it was 0.277 when utilizing EBSD technique. For compressive zone, fractions of α'-martensite were 0.2 and 0.217 obtained from image analysis and EBSD respectively. Hence, the good agreement of the results is an indication of validity of the two employed methods.

3.4. Martensitic transformation quantification

In order to quantify the volume fraction of α'-martensite and investigate its distribution within the bent samples, Olson-Cohen equation

[19] was utilized as follows:

$$f^{\alpha'} = 1 - \exp\{-\beta[1 - exp(-\alpha\varepsilon)]^n\} \qquad (4)$$

where $f^{\alpha'}$ is volume fraction of α'-martensite, α and β are temperature-dependent constants defining the influence of shear bands formation, ε is the imposed strain and n is a constant exponent. For AISI 304L stainless steel, α and β were considered as 3.041 and 3.786 respectively according to the reference [21]. This equation implies that volume fraction of α'-martensite is proportional to the imposed strain. Following the path of the given points, i.e. 1 to 5 illustrated in Fig. 3, the magnitude of the equivalent plastic strain along the cross section of 1.5 mm thick bent samples was obtained and plotted in Fig. 15 using FE results. For all of the V-bent samples, one should notice that, by moving from the compressive zone to the neutral axis of the V-bent samples (i.e. point number 3 at 0.75 mm), the amount of strain reduced. Consequently, according to the Olson-Cohen equation it is expected to have higher amount of α'-martensite in the edges of the bent samples compared to their center. This fact was also shown using optical micrographs illustrated in Fig. 14. Accordingly, by moving from the center of the cross section to the edge of tensile zone, the magnitude of strain increased rapidly and reached to a maximum value at point number 5. Since strain values are larger in tensile zone compared to the compressive zone, the corresponding volume fraction of α'-martensite is expected to be higher as the measured data in Table 4 show. Using the data given in Table 4, and the measured strains for different bent samples, Olson-Cohen equation was plotted for $n = 6$ as shown in Fig. 16.

Exploiting non-destructive magnetic field measurement tests, the amount of α'-martensite which is a ferromagnetic phase was determined for 1.5 mm thick bent samples. Notice that all residual magnetic measurements were carried out at the outer surface of bent samples in the vicinity of point number 5 designated in Fig. 3. Having the volume fraction of α'-martensite and exploiting the results of imposed strain at the tensile stress zone from Fig. 15, the values of residual magnetic field were obtained and correlated to volume fraction of α'-martensite as presented in Fig. 17.

Now by curve fitting on the experimental data for 1.5RD samples, the following empirical equation has been proposed for correlating volume fraction of α'-martensite ($f^{\alpha'}$) and the residual magnetic field (M):

$$f^{\alpha'} = aM + b \qquad (5)$$

where a and b are constants. Their values were found to be 0.46 and -0.48 respectively. Evidently, by increasing the value of residual magnetic field, $f^{\alpha'}$ increases linearly. The significance of this empirical

Table 4
Volume fraction of α'-martensite of 1.5RD V-bent samples.

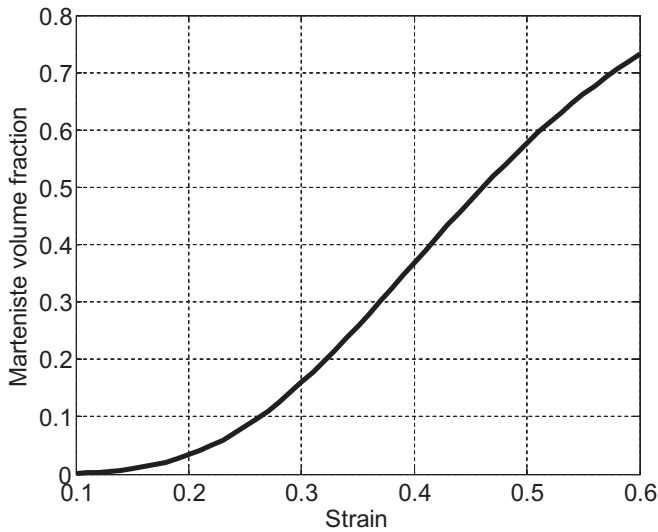| Samples label	1.5RD30	1.5RD45	1.5RD60	1.5RD90
Volume fraction of α'-martensite in tensile zone	0.38	0.29	0.24	0.11
Volume fraction of α'-martensite in compressive zone	0.26	0.2	0.13	0.04

Fig. 16. Variation of martensite volume fraction vs. strain.

Fig. 18. Residual magnetic field for bent samples.

equation is the potential it provides for correlating the residual magnetic field to volume fraction of α'-martensite for different V-bent samples. It should be noticed that, although the suggested empirical equation was attained based on the α'-martensite fraction evaluations and residual magnetic field measurements for 1.5RD samples, owing to the relatively similar trend in reduction of residual magnetic field value for 1.5TD and 1.5QD samples shown in Fig. 18, the equation can also be applied to approximately predict the fraction of α'-martensite within 1.5TD and 1.5QD samples. However, for the other V-bent samples with different thicknesses, the constants of the equation might be different. Results of residual magnetic field measurements for 1.5 mm thick bent samples are given in Fig. 18. These results demonstrate a higher volume fraction of α'-martensite which was formed in rolling direction than those formed in other directions.

The effect of V-bending on micro-hardness of the samples is shown in Fig. 19. This figure shows micro-hardness values reduced by moving from edges of the samples toward the neutral axis. This variation in hardness may be attributed to higher dislocation density together with formation of more α'-martensite in compressive regions of the samples near their edges. These results are consistent with the investigation by Ishimaru et al. [43] examining U-bent parts. In addition, the
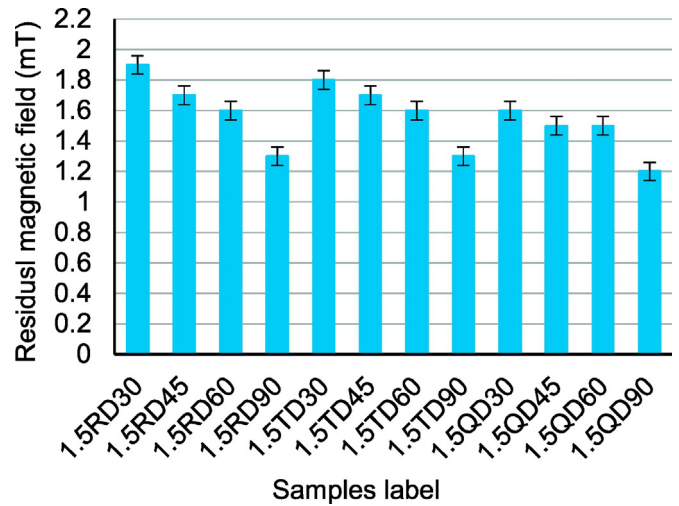
values of hardness can be increased due to more induced plastic deformation when the bending angles are reduced further. The hardness results also indicate that the larger the thickness of the bent sample, the higher volume fraction of transformed α'-martensite and consequently, the higher the value of hardness.

3.5. Final conclusive argument

There is a lack of research work examining the combined influence of V-bending process variables, austenite grain size and orientation, anisotropy parameter and quantification of transformed α'-martensite on spring-forward of austenitic TRIP steels. However, utilizing both macro and micro-scale evaluations in this work, a foundation was made to realize the relationship between texture/microstructural evolution and V-bending behavior of 304L austenitic stainless steel. For this purpose, initially using uniaxial tensile test, the mechanical properties and flow curves of 1.5 mm thick sheets in different cutting directions were determined.

Kermanpur et al. [44] have reported that, deformation mechanism of austenitic stainless steel is mainly controlled by martensitic phase transformation during forming processes. Therefore, since the composition, grain size and thickness of specimens subjected to uniaxial tensile test were taken the same, the anisotropy parameter can affect the flow
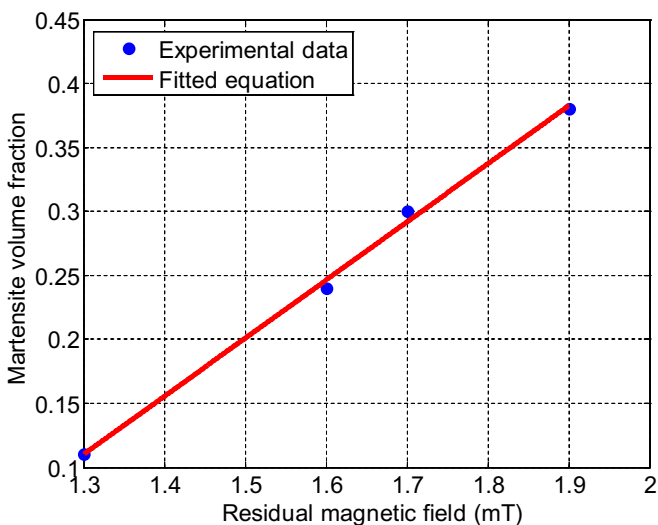

Fig. 17. Curve fitting on experimental data for martensite volume fraction vs. residual magnetic field.
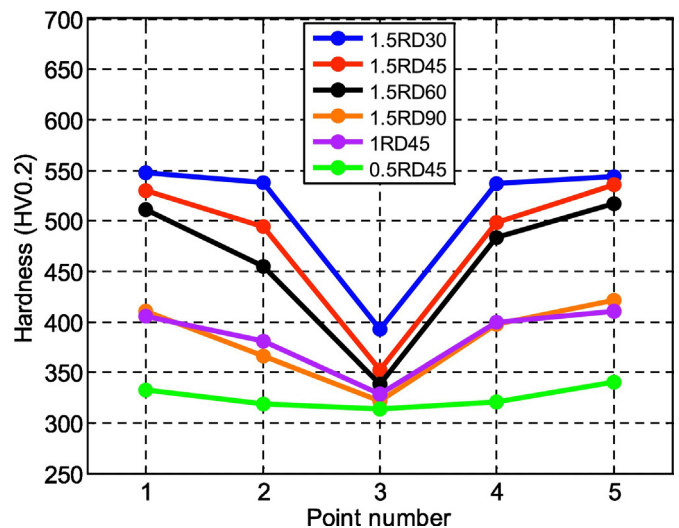

Fig. 19. Variation of Vickers micro-hardness of bent samples along the cross section.

curve behavior presented in Fig. 4. Consequently, based on this figure, it can be concluded that since the extent of austenite to α′-martensite transformation was higher for RD sample, one can expect that its flow curve locates above those of TD and QD specimens. Similar results have been also reported by Beese and Mohr [45]. The significant point provided in Fig. 11 is that, generally the amount of spring forward decreased by increasing value of anisotropy parameter (R-value) when other factors were kept the same. This means 1.5RD samples experienced higher amount of spring-forward in comparison with 1.5TD and 1.5QD samples. Furthermore, as presented in Fig. 18 and 1.5RD samples revealed higher value of residual magnetic field compared to 1.5TD and 1.5QD specimens which is a conclusive indication of higher volume fraction of α′-martensite (see also Fig. 17). On the basis of the mentioned evidences, higher amount of transformed α′-martensite resulted in higher value of spring-forward (i.e. lower spring-back) within the V-bent samples. Therefore, one can claim that by controlling the factors affecting extent of martensitic transformation in TRIP steels including composition and initial austenite grain size and orientation, it is possible to control spring-forward phenomenon in V-bending experiments. According to the aforementioned texture evolution results provided in Section 3.3, finer and more frequent desirable orientations of austenite grains in tensile stress zone can facilitate the martensitic transformation. Thus, it is expected that by performing V-bending operations on the sheets containing coarser grains in the microstructure, volume fraction of α′-martensite diminishes, leading to lower amount of spring-forward.

From another point of view, based on the microstructural and micro-hardness experiments conducted in this study, the tensile and compressive stress zones contributed dominantly for austenite to α′-martensite phase transformation compared to middle region of the V-bent samples. Correspondingly, Wang et al. [46] utilized this perspective to study the influence of neutral axis region shift on spring-back of magnesium sheet comprising twinning. Thus, one can say that by modulating these regions mechanically and metallurgically, it is anticipated to advance the control over the spring-back/forward phenomenon in TRIP steel bent parts.

4. Conclusions

In this study, a comprehensive experimental and finite element analysis of V-bending tests was performed on AISI 304L stainless steel sheets utilizing a novel V-bending die. Based on the attained results, the following conclusions can be derived:

- The anisotropy parameters of the RD, TD and QD samples were determined as 0.81, 0.85 and 0.92 respectively by exploiting a precise digital image correlation (DIC) method coupled with uniaxial tensile test.
- V-bending tests revealed that bent samples exhibited spring-forward phenomenon which increased by reducing bending angle, anisotropy parameter and increasing sample thickness. Spring-forward was also predicted by means of implementing mechanical properties obtained by uniaxial tensile test into finite element analysis.
- EBSD analysis showed that volume fraction of α′-martensite was influenced by the mode of deformation (stress state) within the bent samples, i.e. in tensile stress zone, austenite to α′-martensite transformation occurred at higher amount due to smaller austenite parent grains and more favored orientations in comparison with compressive stress zone which exhibited elongated austenite grains.
- Utilizing micro-hardness tests and microstructural characterizations, it was revealed that austenite to α′-martensite phase transformation occurred dominantly at the edges of bent samples and increased by lowering bending angle and increasing samples thickness.
- The value of spring-forward increased by raising the amount of transformed α′-martensite within V-bent samples. RD samples with lower anisotropy parameter exhibited higher amount of α′-martensite and spring-forward compared to TD and QD specimens. It was suggested that, by modulating parameters affecting deformation-induced martensitic transformation including anisotropy parameter, austenite grain size and orientation, it is possible to control the extent of spring-forward in TRIP steel V-bent parts.
- An empirical equation was proposed to correlate values of residual magnetic field to volume fraction of transformed α′-martensite in V-bent samples.

References

[1] M. Bakhshi-Jooybari, B. Rahmani, V. Daeezadeh, A. Gorji, The study of spring-back of CK67 steel sheet in V-die and U-die bending processes, Mater. Des. 30 (2009) 2410–2419.
[2] D. Hakan, Ö. Mustafa, S. Murat, Effects of material properties and punch tip radius on spring-forward in 90° V bending processes, J. Iron Steel Res. Int. 20 (2013) 64–69.
[3] K.D. Kumar, K. Appukuttan, V. Neelakantha, P.S. Naik, Experimental determination of spring back and thinning effect of aluminum sheet metal during L-bending operation, Mater. Des. 56 (2014) 613–619.
[4] D.-K. Leu, Position deviation and springback in V-die bending process with asymmetric dies, Int. J. Adv. Manuf. Technol. 79 (2015) 1095–1108.
[5] Ö. Tekaslan, N. Gerger, U. Şeker, Determination of spring-back of stainless steel sheet metal in "V" bending dies, Mater. Des. 29 (2008) 1043–1050.
[6] R.H. Wagoner, H. Lim, M.-G. Lee, Advanced issues in springback, Int. J. Plast. 45 (2013) 3–20.
[7] B. Grizelj, J. Cumin, D. Grizelj, Effect of spring-back and spring-forward in V-die bending of St1403 sheet metal plates, Strojarstvo 52 (2010) 181–186.
[8] B. Levy, Empirically derived equations for predicting springback in bending, J. Appl. Metalwork. 3 (1984) 135–141.
[9] L. Zhang, G. Lu, S. Leong, V-shaped sheet forming by deformable punches, J. Mater. Process. Technol. 63 (1997) 134–139.
[10] W. Chan, H. Chew, H. Lee, B. Cheok, Finite element analysis of spring-back of V-bending sheet metal forming processes, J. Mater. Process. Technol. 148 (2004) 15–24.
[11] S. Thipprakmas, Finite element analysis of sided coined-bead technique in precision V-bending process, Int. J. Adv. Manuf. Technol. 65 (2013) 679–688.
[12] S. Chatti, R. Fathallah, A study of the variations in elastic modulus and its effect on springback prediction, Int. J. Mater. Form. 7 (2014) 19–29.
[13] N. Duc-Toan, Y. Seung-Han, J. Dong-Won, B. Tien-Long, K. Young-Suk, A study on material modeling to predict spring-back in V-bending of AZ31 magnesium alloy sheet at various temperatures, Int. J. Adv. Manuf. Technol. 62 (2012) 551–562.
[14] H. Fathi, E. Emadoddin, H.M. Semnani, B.M. Sadeghi, Effect of punch speed on the formability behavior of austenitic stainless steel type 304L, Met. Mater. Int. 22 (2016) 397–406.
[15] K.H. Lo, C.H. Shek, J. Lai, Recent developments in stainless steels, Mater. Sci. Eng. R. Rep. 65 (2009) 39–104.
[16] Y. Xiong, T. He, J. Wang, Y. Lu, L. Chen, F. Ren, Y. Liu, A.A. Volinsky, Cryorolling effect on microstructure and mechanical properties of Fe–25Cr–20Ni austenitic stainless steel, Mater. Des. 88 (2015) 398–405.
[17] N. Li, Y. Wang, W. Liu, Z. An, J. Liu, R. Su, J. Li, P. Liaw, In situ X-ray microdiffraction study of deformation-induced phase transformation in 304 austenitic stainless steel, Acta Mater. 64 (2014) 12–23.
[18] A.F. Padilha, P. Rios, Decomposition of austenite in austenitic stainless steels, ISIJ Int. 42 (2002) 325–327.
[19] G. Olsen, M. Cohen, Kinetics of strain induced martensite nucleation, Metall. Trans. A. 6 (1975) 791.
[20] M.B. Karimi, A. Arabi, A. Khosravani, J. Samei, Effect of rolling strain on transformation induced plasticity of austenite to martensite in a high-alloy austenitic steel, J. Mater. Process. Technol. 203 (2008) 349–354.
[21] A. Hedayati, A. Najafizadeh, A. Kermanpur, F. Forouzan, The effect of cold rolling regime on microstructure and mechanical properties of AISI 304L stainless steel, J. Mater. Process. Technol. 210 (2010) 1017–1022.
[22] H. Wang, Y. Jeong, B. Clausen, Y. Liu, R. McCabe, F. Barlat, C. Tomé, Effect of martensitic phase transformation on the behavior of 304 austenitic stainless steel under tension, Mater. Sci. Eng. A 649 (2016) 174–183.
[23] D. Fei, P. Hodgson, Experimental and numerical studies of springback in air v-bending process for cold rolled TRIP steels, Nucl. Eng. Des. 236 (2006) 1847–1851.
[24] T. Shan, S. Li, W. Zhang, Z. Xu, Prediction of martensitic transformation and deformation behavior in the TRIP steel sheet forming, Mater. Des. 29 (2008) 1810–1816.
[25] S. Kim, Y. Lee, Effect of retained austenite phase on springback of cold-rolled TRIP steel sheets, Mater. Sci. Eng. A 530 (2011) 218–224.
[26] E. ASTM, Standard test methods for tension testing of metallic materials, Annual Book of ASTM Standards, ASTM, 2001.

[27] B. Davoodi, B. Zareh-Desari, Assessment of forming parameters influencing spring-back in multi-point forming process: a comprehensive experimental and numerical study, Mater. Des. 59 (2014) 103–114.

[28] W.F. Hosford, R.M. Caddell, Metal Forming: Mechanics and Metallurgy, Cambridge University Press, 2011.

[29] K. Singh, Strain hardening behaviour of 316L austenitic stainless steel, Mater. Sci. Technol. 20 (2004) 1134–1142.

[30] J.H. Hollomon, Tensile deformation, AIME Trans 12 (1945) 1–22.

[31] P. Ludwik, Elemente der technologischen Mechanik, Springer-Verlag, 2013.

[32] S. Kalpakjian, Manufacturing Engineering and Technology, Pearson Education India, 2001.

[33] S. Thipprakmas, W. Phanitwong, Process parameter design of spring-back and spring-go in V-bending process using Taguchi technique, Mater. Des. 32 (2011) 4430–4436.

[34] D.-K. Leu, A simplified approach for distinguishing between spring-back and spring-go in free U-die bending process of SPFC 440 sheets, Mater. Des. 94 (2016) 314–321.

[35] A. Lebedev, V. Kosarchuk, Influence of phase transformations on the mechanical properties of austenitic stainless steels, Int. J. Plast. 16 (2000) 749–767.

[36] G. Scatigno, M. Ryan, F. Giuliani, M. Wenman, The effect of prior cold work on the chloride stress corrosion cracking of 304L austenitic stainless steel under atmospheric conditions, Mater. Sci. Eng. A 668 (2016) 20–29.

[37] N. Gey, B. Petit, M. Humbert, Electron backscattered diffraction study of ε/α' martensitic variants induced by plastic deformation in 304 stainless steel, Metall. Mater. Trans. A 36 (2005) 3291–3299.

[38] S. Kundu, H. Bhadeshia, Transformation texture in deformed stainless steel, Scr. Mater. 55 (2006) 779–781.

[39] S.J. Lee, Y.K. Lee, Effect of austenite grain size on martensitic transformation of a low alloy steel, Materials Science Forum, Trans Tech Publ, 2005, pp. 3169–3172.

[40] Y.B. Das, A.N. Forsey, T.H. Simm, K.M. Perkins, M.E. Fitzpatrick, S. Gungor, R.J. Moat, In situ observation of strain and phase transformation in plastically deformed 301 austenitic stainless steel, Mater. Des. 112 (2016) 107–116.

[41] A. Tiamiyu, M. Eskandari, M. Nezakat, X. Wang, J. Szpunar, A. Odeshi, A comparative study of the compressive behaviour of AISI 321 austenitic stainless steel under quasi-static and dynamic shock loading, Mater. Des. 112 (2016) 309–319.

[42] P.L. Mangonon, G. Thomas, The martensite phases in 304 stainless steel, Metall. Trans. A. 1 (1970) 1577–1586.

[43] E. Ishimaru, H. Hamasaki, F. Yoshida, Deformation-induced martensitic transformation behavior of type 304 stainless steel sheet in draw-bending process, J. Mater. Process. Technol. 223 (2015) 34–38.

[44] A. Kermanpur, P. Behjati, J. Han, A. Najafizadeh, Y. Lee, A microstructural investigation on deformation mechanisms of Fe–18Cr–12Mn–0.05 C metastable austenitic steels containing different amounts of nitrogen, Mater. Des. 82 (2015) 273–280.

[45] A.M. Beese, D. Mohr, Anisotropic plasticity model coupled with Lode angle dependent strain-induced transformation kinetics law, J. Mech. Phys. Solids 60 (2012) 1922–1940.

[46] L. Wang, G. Huang, T. Han, E. Mostaed, F. Pan, M. Vedani, Effect of twinning and detwinning on the spring-back and shift of neutral layer in AZ31 magnesium alloy sheets during V-bend, Mater. Des. 68 (2015) 80–87.